Conformational influence of fluorinated building blocks on the physical properties of polyesters

Sophie Lingier[1], Robert Szpera[2], Bart Goderis[3], Bruno J. Linclau[2], Filip E. Du Prez[1*]

[1] Polymer Chemistry Research Group, Centre of Macromolecular Chemistry (CMaC), Department of Organic and Macromolecular Chemistry, Ghent University, Krijgslaan 281 S4bis, 9000 Ghent, Belgium, *Email corresponding author: Filip.DuPrez@ugent.be
[2] Department of Chemistry, University of Southampton, Highfield, Southampton SO17 1BJ, United Kingdom
[3] Polymer Chemistry and Materials Division, Chemistry Department, KU Leuven, B-3001 Leuven, Belgium

Abstract

The interplay of the relative configuration of diastereomeric vicinal difluoride groups on the conformational properties of polyesters has been investigated and compared to their non-fluorinated and per-fluorinated counterparts. The incorporation of *syn* and *meso* vicinal difluoride units in the polymer backbone was expected to influence the rigidity and stacking behaviour of the polymers in a significant way, and therefore to result in different thermal properties, such as melting point and melting enthalpy. Both *syn* and *meso*-2,3-difluoro butanediol have been reacted with the diester dimethyl succinate, leading to the formation of polyesters that have been characterized with ^{1}H, ^{13}C and ^{19}F NMR. The polyesters showed molar masses up to 20 kg/mol (SEC). Surprisingly, the *syn* and *meso*-polymers displayed identical crystallization and melting behaviour. In contrast, differences were observed in the crystallization kinetics and melting points of *syn* and *meso* oligomers. Relying on time-resolved synchrotron SAXS and WAXD experiments, the complex multiple melting behaviour of these oligomers was explained in terms of crystal size and surface effects. The slower crystallization kinetics for the *meso* oligomers was tentatively associated with a stronger tendency to adopt *gauche* configurations. Apparently, such effects no longer affect the crystallization kinetics when larger polymers crystallize. It was also found that the *syn* and *meso*-polymers have identical equilibrium melting points and melting enthalpies notwithstanding molecular and crystallographic differences.

Keywords: polyesters, fluorinated building blocks, diastereoisomers

Introduction

For years there has been great interest in polymers containing fluorine atoms. As a result of their fluorinated nature, these polymers show a low surface energy, good thermal stability, excellent dielectric properties, good chemical resistance, low water absorption, and high weatherability.[1] The most well-known example is polytetrafluoroethylene (PTFE), which is used today in a vast variety of applications.[2] Fluorine functionalities were also incorporated in other classes of polymers such as polyurethanes and polyacrylates in order to alter their properties.[3-6] In addition, fluoroaliphatic polyesters have the potential for yielding new and interesting materials, since it can be anticipated that these polymers would possess some of the special properties of PTFE.[7]

In contrast to for example the class of polyurethanes, hydrogen bonding is less pronounced in polyesters, which facilitates the investigation of the effect of the presence of fluorine atoms in the backbone on the resulting polymer properties. Yet, up until now, only a few examples of fluoroaliphatic polyesters were reported, presumably due to the challenges associated with the synthesis of fluorinated monomers or with the actual polyester synthesis.[8-10] Because hydrolytically unstable polymers are obtained when fluorinated dicarboxylic acid derivatives are used, it is crucial to introduce fluorination in the diol monomer.[11] However, the inductive effect of the fluorine atoms renders the alcohol groups less nucleophilic, causing a lower reactivity in esterification reactions and thus the formation of oligomers, rather than high molecular weight polymers.[12]

So far, only fluoroaliphatic polyesters containing CF_2 units in the main chain are reported,[8-10] while, to the best of our knowledge, polyesters containing CHF units have never been described. Yet, these polyesters may show interesting properties as such units result in stereocentres along the polymer backbone. In general, many polymers prepared by coordination polymerization, such as the commodity polymer polypropylene, show stereoisomerism and have been investigated and industrially produced since many decades. The effect of stereochemistry along the polymer backbone on for example the packing of polymer chains, and the resulting thermal and mechanical properties has therefore been investigated intensively.[13-15].

It is known that two adjacent stereogenic CHF units reduce conformational flexibility around their common C-C bond, due to a $\sigma_{CH} \rightarrow \sigma^*_{CF}$ hyperconjugation effect. This effect is maximal when the C–H and C–F bonds adopt an antiperiplanar orientation.[16-17] In 1,2-difluoroethane, this effect results in the conformation in which the two fluorine atoms adopt a *gauche* conformation being more stabilised compared to the *anti*-conformer.[18-22] Hence, The vicinal difluorinated motif offers opportunities for conformational control based on the *gauche* effect, when introduced in a longer chain. The introduction of this motif within a longer alkyl chain gives rise to two stereocentres, with *syn* or *anti* relative stereochemistry. Hence, the conformational landscape of such difluorinated chains is perturbed compared to the non-fluorinated chain, with the *gauche* effect now being one of the factors that determines conformer stability.[23] With a different relative vicinal difluoride stereochemistry, a different set of conformer populations is thus obtained. However, the *gauche* effect is not a very strong effect, and it has been shown that for the 2,3-difluorobutane diastereomers, steric and dipole effects also contribute significantly to the overall conformer population.[23] Nevertheless, the introduction of vicinal difluorides within long alkane chains including fatty acids and cycloalkanes was shown to result in a dramatic difference in melting point between the two diastereomers.[24-27] In addition, the introduction of this motif in bioactive compounds has been exploited as a conformational control element, targeted at promoting the population of bioactive conformations,[16] materials[28-29] or organocatalysts.[16, 30-33]

In this study, the interplay of the relative configuration of isomeric vicinal difluoride groups on the conformational properties of polyesters is compared to the non-fluorinated and per-fluorinated counterparts. In this context, it will be investigated if the incorporation of *syn* and *meso* vicinal difluoride units in the polymer backbone influences the rigidity and stacking behaviour of the polyesters in a significant way because this could result in different crystallization behaviour for example.

In order to investigate this, the starting point of this study was the synthesis of a polymerizable diol monomer containing a vicinal difluoride unit. Racemic *syn* and *meso* 2,3-difluoro butanediol were chosen as monomers, since the synthesis of these monomers was previously reported by Linclau and coworkers.[34-35] In order to maximize the influence of the configuration and conformation of these monomers on the resulting polymer properties, dimethyl succinate, which is a diester with a short carbon chain (C4), was chosen as the comonomer in a polycondensation based on a transesterification process (Scheme 1).[36-39]

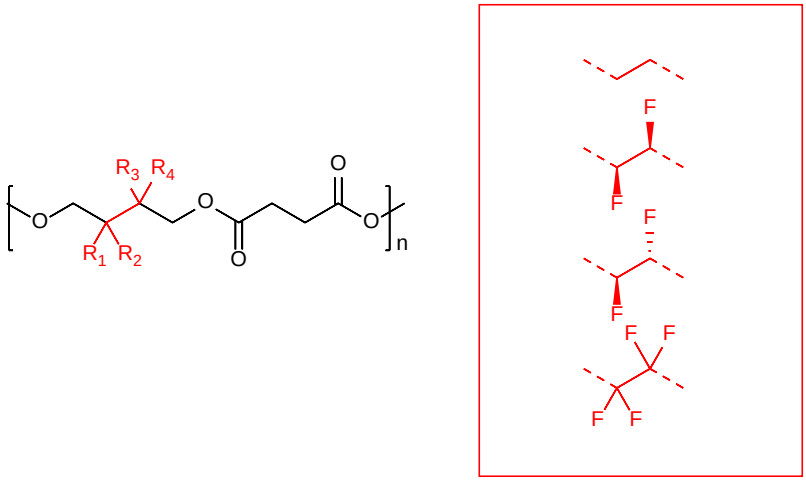

Scheme 1. Overall scheme of the four different polymers that were prepared and investigated.

For the series of fluorinated polyesters and the corresponding non-fluorinated version (polybutylene succinate, PBS), the polycondensation was optimized to yield high molecular weight polymers. Subsequently, the thermal properties, such as degradation temperature, melting point and melting enthalpy were determined. Finally, the thermal behaviour of the polyesters in relation to their semi-crystalline structure was thoroughly investigated using time-resolved synchrotron SAXS and WAXD.

Experimental

Materials

2-Butanone, dichloroethane (99.8+%) and dimethyl formamide (extra pure) were purchased from Acros Organics. 1,4-Butanediol (99%), chloroform (≥99.8%), dimethyl acetamide, dimethyl succinate (98%), methanol (≥99.9%) and methyl sulfoxide (99.8+%) were purchased from Sigma-Aldrich. Tetrabutyl orthotitanate and 2,2,3,3-tetrafluoro-1,4-butanediol (>95%) were purchased from TCI. Chloroform-*d* ($CDCl_3$, Euriso-Top, 99.8%), dimethylsulfoxide-d_6 (Euriso-Top, 99.8%), dibutyltin oxide (DBTO, Janssen Chimica, 98%), iso-propanol (Chem-lab, 99+%), tetrahydrofuran (Fisher Chemical, analytical reagent grade) and all previously mentioned substances were used as received. The synthesis of *meso*-2,3-difluoro-1,4-butanediol and *rac-syn*-2,3-difluoro-1,4-butanediol was performed as reported.[35]

Instrumentation

Size exclusion chromatography (SEC) measurements were performed on a Waters instrument, equipped with 3 Polymer Standards Services GPC serial columns (1 X GRAM Analytical 30Å, 10µm and 2 x GRAM Analytical 1000Å, 10µm) at 35 °C with a RI detector (2414 Waters). PMMA standards were used for calibration and DMA containing LiBr (0.42 g mL^{-1}) was used as a solvent at a flow rate of 1ml min^{-1}. Molecular weights and dispersities were determined using Empower software. SEC-measurements were also performed on a Waters instrument, equipped with Waters Styragel HR3, HR4 and HR5 serial columns (5µm particle size) at 35 °C with a RI detector (2410 Waters), using PS standards for calibration, and $CHCl_3$

as an eluent at a flow rate of 1.0ml min^{-1}. Molecular weights and dispersities were determined using the Breeze Millennium software. *^{1}H, ^{13}C and ^{19}F-NMR spectra* were recorded on a Bruker Avance 300 and a Bruker Avance 500 (at 300 MHZ and 500MHz respectively for ^{1}H NMR; 75 MHZ and 125MHz respectively for ^{13}C NMR; and at 282MHz and 470MHZ respectively for ^{19}F NMR). Chemical shifts are presented in parts per million (δ) relative to DMSO-d_6 or $CHCl_3$-*d* (2.50 ppm or 7.27 ppm in ^{1}H- and 39.51 ppm or 77.24 ppm in ^{13}C-NMR respectively) as internal standard. All measurements were performed at 25 °C and ACD/NMR Processor was used for the processing of all data. *Differential scanning calorimetry (DSC)* was performed with a Mettler Toledo instrument 1/700 under nitrogen atmosphere. Experiments were composed of (first) heating, cooling and second heating runs all at 10°C/min between 0°C or 25°C and 200°C or 250°C, depending on the sample. For the polyesters derived from *meso* and *rac-syn* 2,3-fluorobutanediol, the experiments were conducted in a TA Instrument Q2000 DSC under similar conditions between -10°C and 170°C. *LC-MS analyses* were performed on an Agilent Technologies 1100 series LC/MSD system with a diode array detector (DAD) and a single quad MS. *Thermogravimetric analyses (TGA)* were performed with a Mettler Toledo TGA/SDTA851e instrument under nitrogen atmosphere at a heating rate of 10 °C min^{-1} from 25 °C to 800 °C. *Time-resolved synchrotron X-ray experiments* were performed at DUBBLE, the Dutch-Belgian beamline (BM26) at the European Synchrotron Radiation Facility (ESRF; Grenoble, France). *Small-angle X-ray scattering (SAXS) and wide-angle X-ray diffraction (WAXD)* patterns were recorded simultaneously using a wavelength, λ, of 1.033 Å. The SAXS signals were collected on a two-dimensional Pilatus 1 M detector at 3 m from the sample after an evacuated tube. A Pilatus 300 K detector positioned close to the sample, was used for recording the WAXD data. The scattering angles were calibrated with silver behenate and high-density polyethylene standards.

Methods

Polyester synthesis

PBS. A Schlenk tube was filled with 2.00 g (1.0 eq) dimethyl succinate, 1.38 g (1.1 eq) 1,4-butanediol and 0.02 g (0.6 mol%) DBTO. The tube was flushed (3X) with N_2 at room temperature. Next, the reaction mixture was heated to 160 °C for 2.5 h followed by 0.5 h at 180 °C. Then, vacuum of one mbar was applied and the reaction was kept like this for 3.5h. Hereafter, the reaction was cooled to room temperature and brought to atmospheric pressure under N_2 gas. The polymer was dissolved in chloroform and precipitated in cold methanol. The precipitate was filtered off and washed with methanol. Finally, the polymer was dried under vacuum at 40 °C.

Fluorinated polymers. A Schlenk tube was filled with 1.0 eq dimethyl succinate, 1.1 eq fluorinated diol and 0.6 mol% DBTO. The tube was flushed (3X) with N_2 at room temperature. Next, the reaction mixture was heated to 160 °C for 4 h. The temperature was raised to 180 °C and for one hour the pressure was lowered to 200 mbar. After this, the vacuum was lowered to one mbar and the mixture was stirred as such for 3.5 h. Hereafter, the reaction was cooled to room temperature and brought to atmospheric pressure under N_2 gas. The polymer was dissolved in dimethyl formamide and precipitated in cold methanol. The precipitate was filtered off and washed with methanol. Finally, after being dried under vacuum at 40 °C, the polymer was obtained as a white powder.
Note: The fluorinated oligomers have been prepared using 1 equivalent of the fluorinated diol. The reaction were carried out in inappropriate 100mL Schlenk flasks, which led to a nonhomogeneous polymerization

medium with some of the melt sticking to the flask. Therefore, the polymerization conditions were improved by the use of Schlenk tubes, leading to higher molecular weight polymers.

SAXS and WAXD experimental method can be found in SI 3.1.

Results and discussion

Monomers

Two vicinal difluoro containing diols (Figure 1) having a different relative configuration were prepared via a literature procedure.[35] The *meso* compound is achiral, while the *syn*-2,3-difluoro butane diol was synthesized as a racemic mixture.

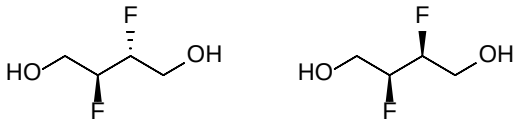

Figure 1. Structures of *meso* and (racemic) *syn* 2,3-difluoro butane diol.

Synthesis of the polyesters (Scheme 2)

Initially, PBS was synthesized prior to the polymerization of the fluorine containing butane diols with dimethyl succinate. Two different polymerization methods were tested in which butanediol was combined with dimethyl succinate or with succinoyl chloride. First, polyesters were made from 1,4-butanediol and dimethyl succinate. The procedure used was repeated from literature and was performed on a scale of 2.5 g of diester with DBTO as the catalyst.[38] High molecular weight polyesters of up to 22 kDa were obtained, which were used as a reference sample for all fluorine containing polymers afterwards. Anyhow, 1,4-butanediol was also combined with succinoyl chloride to investigate if this method results in high molecular weight polymers. When working with acid chlorides, high temperatures and mechanical stirring are not necessary, making this a milder method. However, in compared to the first method, a doubling of the reaction time is necessary and only low molecular weight polymers (M_n < 6 kDa) were obtained.

2,2,3,3-Tetrafluoro-1,4-butanediol is a readily available diol, which was first applied in the polymerization process with dimethyl succinate before using the small scale 2,3-difluoro-1.4-butanediol compounds. First, only low molecular weight products were obtained as a result of the known effect that the fluorine groups are electron-withdrawing groups leading to reduced nucleophilicity of the hydroxyl groups.[11] Moreover, as the fluorinated diol showed to be more volatile than 1,4-butanediol, an additional step had to be added to avoid evaporation of the diol early in the polycondensation reaction. After 3 h of transesterification, 1 h of polycondensation at low vacuum (200 mbar) was inserted in the polymerization schedule, which still resulted in oligomers (Table 3).

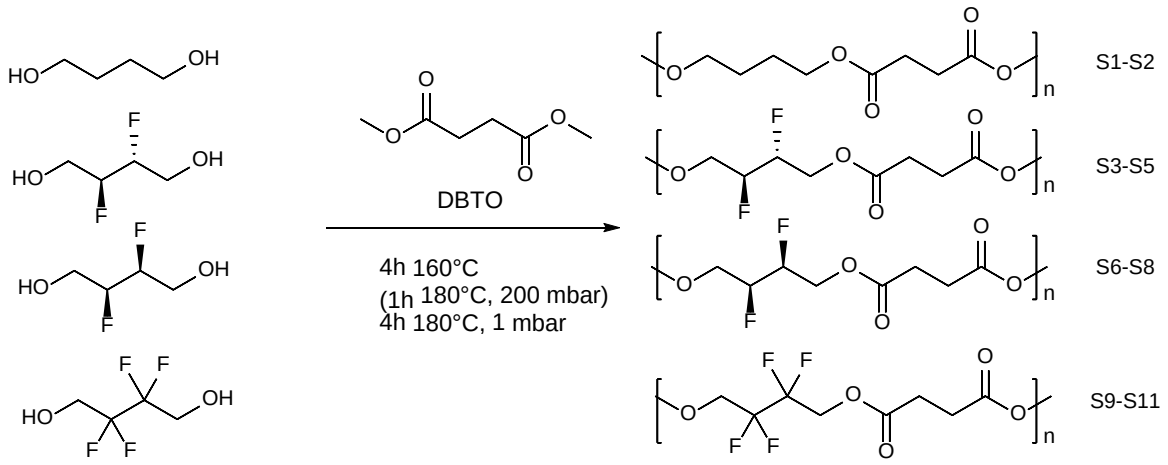

Scheme 2. Overview of the synthesis of four polyesters based on butane diol, *meso*- and *rac-syn*-2,3-difluorobutane diol and 2,2,3,3-tetrafluoro-1,4-butane diol.

In an attempt to achieve higher molecular weights, the catalyst and polymerization method was varied. First, titanium butoxide was tested as a catalyst instead of dibutyl tin oxide but higher molecular weights were again not obtained.[37] Then, the set-up was changed to avoid sticking of compounds to the edges of the 100 ml round bottom flask and thus having deviations from stoichiometry.[40] Instead of using a 100 ml round bottom flask, a high-pressure 50 ml 2-neck tube was used with a mechanical stirrer adjusted to this set-up. An improvement in the stirring of the mixture could be observed, resulting in higher molecular weight polymers (Table 1). This optimized set-up and procedure with DBTO as the catalyst was then used for the polymerization of *syn* and *meso* 2,3-butanediol with dimethyl succinate.

Table 1. Overview of the SEC, TGA and DSC (second heating) results of the synthesized polymers

Diol used in polymerization	M_n[a] (kDa)	M_n[b] (kDa)	Đ[b]	T_d (°C)	T_m (°C)	ΔH (J/g)
1,4-butanediol	-	22	1.6	300	116	54
Meso-2,3-butanediol	27	30	1.9	310	114 & 124	42
Rac-syn-2,3-butanediol	21	25	2.1	320	114 & 124	42
2,2,3,3-tetrafluoro-1,4-butane diol	29	18	1.7	295	77 & 93	35

[a] M_n obtained from end-group analysis from ^{1}H-NMR

[b] M_n and Đ obtained from SEC analysis.

Molecular weights were obtained from SEC-analysis in chloroform for PBS and in DMA for the fluorine containing polymers. High molecular weights were obtained (M_n > 20 kDa), which were also confirmed by end group analysis in NMR. The chemical structures of the polymers were confirmed with ^{1}H, ^{13}C and ^{19}F NMR measurements (Figure S1-S10).

Solubility

To investigate the solubility, 0.01 g of polymer was transferred in a 1 mL solution of seven different solvents (Table 2). PBS was only soluble in chloroform while poly(2,3-difluorobutylene succinate) was only soluble in high boiling solvents like DMSO, DMF and DMA. Poly(2,2,3,3-tetrafluorobutylene succinate) showed the highest solubility.

Table 2. Overview of the solubility of the polyesters in organic solvents

Diol used in polymerization	$CHCl_3$	DCE	THF	MEK	DMA	DMF	DMSO
Butane diol	+	-	-	-	-	-	-
Meso-2,3-butanediol	-	-	-	-	+	+	+
Rac-syn-2,3-butanediol	-	-	-	-	+	+	+
2,2,3,3-tetrafluoro-1,4-butane diol	±	-	+	+	+	+	+

Thermal analysis

TGA analysis showed a degradation temperature at 5% mass loss of around 300 °C for all polymers. On the other hand, DSC analysis displayed the semi-crystalline nature of all polymers (Figure S11-S12). PBS shows the highest melting enthalpy during second heating (54 J/g) while the introduction of fluorine atoms significantly reduces the melting enthalpy (Table 1). While this observation was expected because their introduction makes the stacking less close compared to the aliphatic chain in PBS, it was against our expectations that the *meso*- and *syn*-butane diol derived polymers show the same melting points and melting enthalpies. In fact, the crystallization kinetics during cooling as well as the thermal behaviour during heating for these two polymers are virtually identical (Figure S-12). This also holds for the glass transition temperatures, seen in both cases as a step like transition at about 14°C in the DSC traces (Figure S-12). On the other hand, as observed from Table 3, the DSC measurements (second heating runs, Figure S13) of the *meso* and *syn* oligomers, obtained at the start of this study, displayed lower melting points and enthalpies than their polymeric analogues. In fact, the *meso* oligomers do not crystallize during cooling (Figure S-14) whereas the *syn* oligomers do (Figure S-15). The zero enthalpy value reported in Table 3 for the *meso* oligomer during heating result from the superposition of exothermic heat due to (cold) crystallization taking place just before melting. The associated endothermic melting enthalpy fully compensates the crystallization heat (Figure S-14). The melting point for the *meso* oligomer was taken at the endothermic peak maximum. To explain these differences in thermal behaviour, an extensive time-resolved SAXS/WAXD analysis (*vide infra*) was performed on oligomers of the *meso* and *syn* poly(2,3-difluorobutane succinate) during first heating, subsequent cooling and second heating.

Table 3. Overview of the SEC and DSC (second heating run) measurements on oligomers and polymers derived from *meso* and *syn*-2,3-butanediol.

Diol used in polymerization	M_n (kDa)	Đ	T_m (°C)	ΔH (J/g)
Meso-2,3-butanediol	5.3	1.2	89	0
Meso-2,3-butanediol	30	1.9	114 & 124	42
Rac-syn-2,3-butanediol	2.5	1.3	104 & 116	32
Rac-syn-2,3-butanediol	25	2.1	114 & 124	42

X-ray diffraction measurements

As the *meso* and *syn* oligomers presented in Table 3 showed different DSC traces with a large difference in melting points and enthalpy, it was decided to investigate this more thoroughly. During second heating, the *meso* oligomer shows a single low melting point (89 °C) due to the melting of crystals which were formed during the heating run, while the *syn* oligomer has two melting points (117 and 124 °C) related to crystals formed during the preceding cooling run. The associated melting enthalpy is rather large (32 J/g) (Table 3).

In order to investigate this difference in crystallization and melting behavior, small-angle X-ray scattering (SAXS) and wide-angle X-ray diffraction (WAXD) measurements were performed.

The WAXD data for the *meso* oligomer (Figure 2 left, S16-S19) reveals that all crystals during the first heating, subsequent cooling and second heating, have an identical internal structure because when structures melt or crystallize, the WAXD crystalline reflections decrease or increase in intensity but do not alter in position (except for minor changes related to thermal expansion) or relative intensities. The vertical lines represent melting onsets for folded chain lamellar crystals with a thickness given by the discrete number of molecular repeats as indicated. These lines could be inserted after SAXS measurements. The transitions in Figure 2 can be related to the DSC transitions of the respective oligomer. When comparing Figure 2 (left) to the DSC of the *meso* oligomer in Figure S14, the same three melting points could be observed during first heating. In the cooling, no transition was observed in DSC which is also reflected in the zero values in the WAXD crystalline mass fraction (Figure 2, left), proving that the crystallinity remains zero at any temperature during cooling. For the second heating, DSC suggested cold crystallization and subsequent melting, which is clearly seen in the rise and fall of the WAXD crystallinity during second heating. The 4 step like melting transitions shown in Figure 2 (right) for the *syn* oligomer during first heating and the three melting points during second heating are not clearly reproduced in the DSC data (Figure S15), likely because the high temperature melting events overlap. For the *syn* oligomer, the cooling leads to crystallization, in contrast to for the *meso* oligomer. Note that he *syn* oligomer crystal structure is different from that of the *meso* sample as expected because of the difference in relative configuration of the vicinal fluorines along the backbone. This difference is reflected in differences in the positions of the WAXD crystalline reflections (Figures S16-S19).

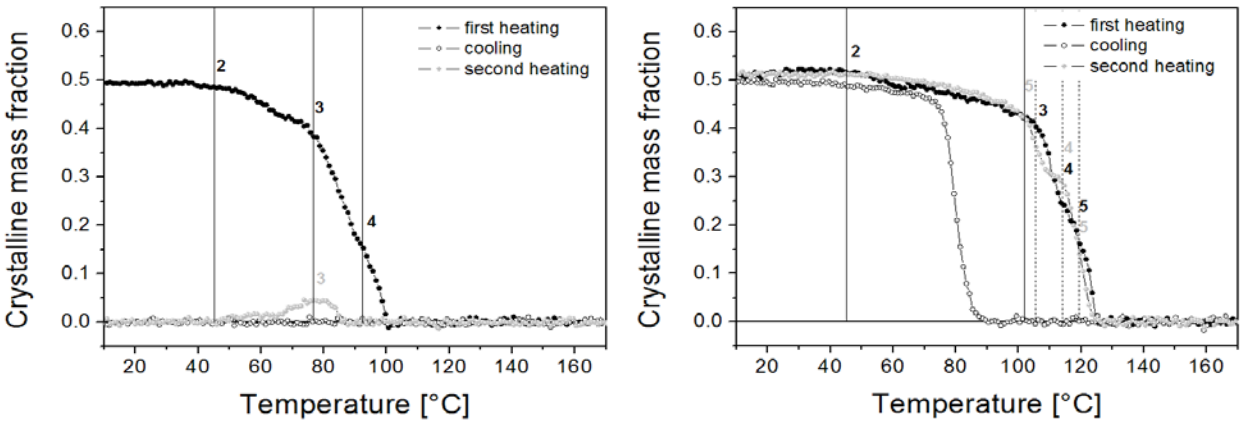

Figure 2. WAXD based crystallinity for the *meso* (left) and *syn* (right) oligomer. Vertical lines represent melting onsets for folded chain lamellar crystals with a thickness given by the discrete number of molecular repeat units as indicated. Full lines correspond to the melting of folded chain crystals whereas the dashed lines represent the melting onsets of extended chain crystals. The black numbers indicate that these crystals types were present in the sample that was heated first. Grey numbers indicate that these crystal types were present in the sample that was subjected to the second heating run.

The SAXS patterns of the *meso* oligomer (Figure 3, top) prior to heating exhibit two (non-crystallographically related) scattering maxima, reflecting the presence of two different semi-crystalline stacks with different periodicity. The crystals that melt at the lowest temperature are partially contained in the stacks that produce a SAXS maximum at high angles as this maximum disappears upon melting. However, the fact that also the low angle peak shifts to lower values, indicates that some of the thinnest crystals are also present in stacks where the thicker crystals reside. Indeed, when some of the thinnest crystals melt in these stacks, the intercrystallite separation should increase and hence also the average

periodicity in the stack. It seems that the intermediate and high temperature melting crystals are contained within the same stacks because, upon melting of the intermediate crystals at about 80 °C, the remaining low angle peak shifts to lower angles. Furthermore, the increased declining scattering from the origin reflects the increased presence of isolated lamellar crystallites once the intermediate crystals have melted.

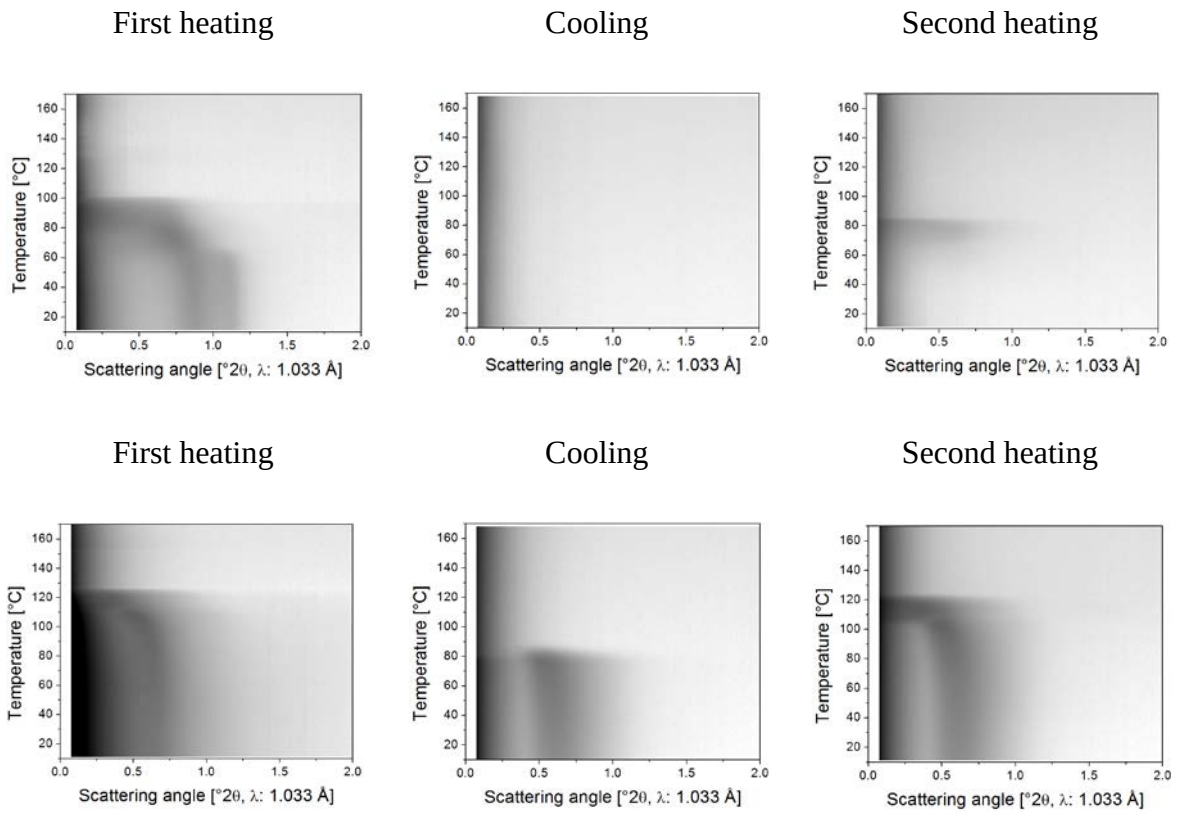

Figure 3. Temperature dependent SAXS patterns for the *meso* (top) and *syn* (bottom) oligomer, seen from the top with the intensities (on a log scale) displayed using grey tones with black and white being high and low intensities.

For the *syn* oligomer, the SAXS patterns (Figure 3 bottom) collected during the first heating seem simpler as only one strong maximum is present. Nevertheless, the stepwise WAXD crystallinity drops (Figure 2 right) reveal the presence of four crystal types, rather than three for the *meso* oligomer. The fact that only one major SAXS peak is observed suggests that all crystals are present in one stack.

In order to determine the thickness of the crystals in the oligomers, the SAXS patterns were interpreted in terms of the Hosemann model for paracrystalline layer stacks.[41] The model as presented in section 3.1. of the supporting info assumes Gaussian thickness distributions of the crystalline and amorphous layers and is not suited to describe SAXS patterns of lamellar stacks that contain discretely different crystal thicknesses. At the highest temperatures, where only one stack of crystals with a certain thickness was remaining, the SAXS pattern could be fitted to the theoretical model. It was found that the SAXS patterns pertaining to the first heating run could not be approached well with Eq. S1 (see supporting info), except at the highest temperatures where only one crystal thickness type was remaining.

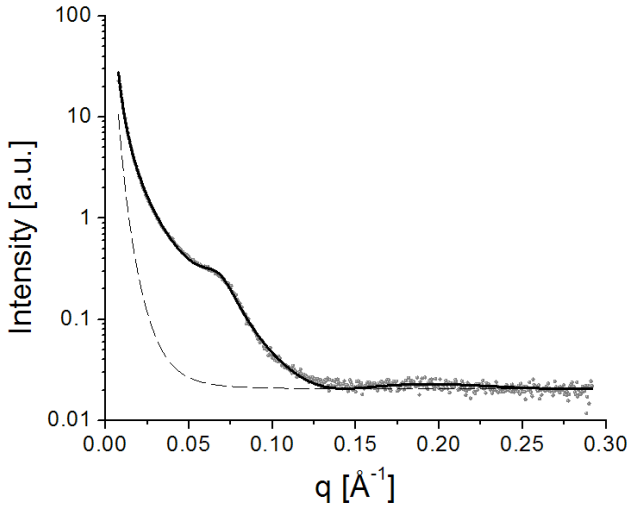

Figure 4. Experimental SAXS pattern collected during the first heating run at 95 °C for the *meso* sample (grey dots). The full curve represents the theoretical pattern resulting from a fit of the experimental data to Eq. S1. The dashed line represents the background share to I(q). The crystal thickness, l_C, equals 43.9 Å, l_A = 41.5 Å, σ_A = 22 Å and α = 0.52. Other parameters are not relevant as they do not describe the semi-crystalline structure.

The result of fitting the pattern of the *meso* oligomer at 95 °C with the model is shown in Figure 4. As only one crystal thickness was present, σ_C was set equal to 1. The thickness of the high melting crystals equals 43.9 Å. Interestingly, all SAXS patterns from the second heating run could be approached very well with Eq. S1 and σ_C = 1. It seems that crystals are formed and disappear with a fixed thickness equal to 31.9 Å. The result of fitting Eq. S1 to the SAXS pattern at 80 °C during the second heating run is shown in Figure S20. The captions to the figures lists all structurally relevant parameters. Note that the melting point of the intermediate crystals in heating run 1 corresponds to the melting point of the crystals that were created during the second heating run, suggesting an equal crystal thickness for this intermediate type of crystals.

Similar as for the *meso* sample, the SAXS patterns for the *syn* oligomer at the highest temperatures for the first heating could be fitted adequately to Eq. S1 (and with σ_C = 1) as illustrated for 122 °C in Figure 5. The thickness of the most stable crystals (i.e. the ones that melt at the highest temperatures) equals 49.1 Å. Fitting to Eq. S1 with σ_C = 1 also worked out for the cooling run at high temperatures, as illustrated for 86 °C in Figure S21. The thickness of the first formed crystals equals 42.6 Å. One may expect that the first formed crystals are the most stable and perfect ones, which should melt at the highest temperatures. The SAXS patterns of the second heating run at the highest temperatures indeed returned similar crystal thickness value, but fitting to Eq. S1 could only be realized with a σ_C significantly larger than 1, suggestion the additional presence of crystals with different thickness. Given the observation that the melting offset during second heating coincides with that of the first heating run, it seems that crystals with a thickness of 49.1 Å (the value found at high temperatures during the first heating run) might also be present to a small amount. These thicker crystals might be generated during the (second) heating run via melting and recrystallization of the thinner crystals.

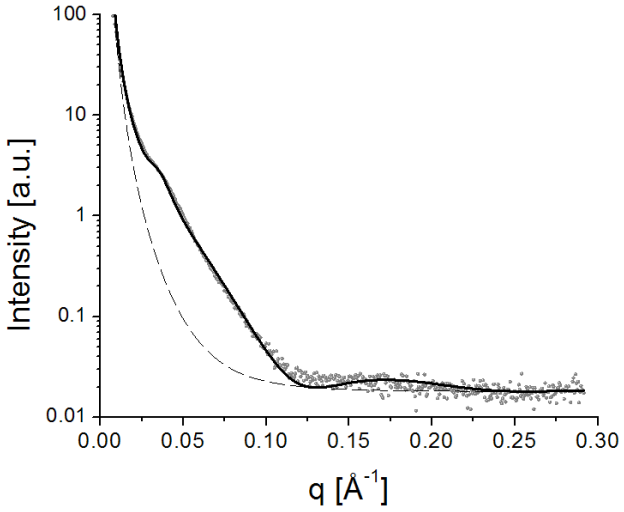

Figure 5. Experimental SAXS pattern collected during the first heating run at 122 °C for the *syn* sample (grey dots). The full curve represents the theoretical pattern resulting from a fit of the experimental data to Eq. S1. The dashed line represents the background share to I(q). The crystal thickness, l_C, equals 49.1 Å, l_A = 107.9 Å, σ_A = 49.0 Å and α = 0.49. Other parameters are not relevant as they do not describe the semi-crystalline structure.

Classically, the melting point of lamellar crystals can be described by means of the Gibbs-Thomson equation:

$$T_m = T_m^0 \left(1 - \frac{2\sigma_e}{\Delta H l_C}\right) \quad (1)$$

This equation implies that plotting the melting point (the melting peak onset is most relevant), T_m, as a function of the inverse lamellar thickness should yield a straight line with an intercept at T_m^0, the equilibrium melting point of crystals that are infinitely thick. In Eq. (1), σ_e is the (fold) surface free energy and ΔH is the theoretical melting enthalpy of 100% crystalline material (not to be confused with the experimental melting enthalpy, which is crystallinity dependent).

When analyzing the crystal thickness values obtained through the fits, it seems that they all can be approximated by an integer (n) times 10.2 Å. This 10.2 Å corresponds to the length of one stretched out molecular repeat, l_R, and the integer number to the number of unit cells along the lamellar thickness direction, assuming that the molecules are configured with their molecular axis perpendicular to the lamellar (fold) surface. In fact, the 10.2 Å was obtained by calculating nl_R=l_C for every experimental value for l_C and by minimizing the squared difference between the calculated and experimental l_C values.

For the *meso* oligomer, most likely three types of crystals are present during the first heating run with each its own characteristic melting point. The three *meso* sample melting points are added to Figure 2 (left), with vertical full lines. The labels on these lines correspond to the number of molecular repeats spanning the thickness of the crystals that are melting once passed the respective melting onset. For the *syn* oligomer, five melting points were found. These melting points were added to Figure 2 with dashed and full vertical lines and labelled with the number of molecular repeats along the crystal thickness.

The as obtained calculated l_C values (for different *n*-values) were inverted to $1/l_C$ and represented in Figure 6 by the vertical dashed lines. To each of the calculated $1/l_C$ values experimentally observed melting points were associated either from the *meso* (open circles in Figure 6) or the *syn* (open diamonds in Figure 6) sample. Except for the crystal thicknesses that were obtained experimentally (full circles for the *meso* sample and full diamonds for the *syn* sample in Figure 6) at the ends of the melting traces, the association of experimental melting points with calculated $1/l_C$ values is of course arbitrary. However, following the Gibbs-Thomson formalism, links should be made to obtain a straight line. After some trials it appeared most consistent that two rather than one linear relationship should be defined - with a common intercept at 139.9 °C - to properly link the experimental melting onsets to crystal thicknesses, i.e. the red and black lines in Figure 6.

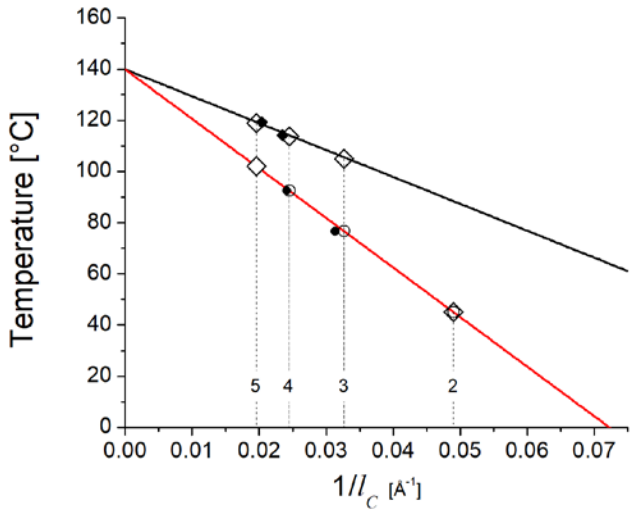

Figure 6. Gibbs Thomson plots relating the inverse crystal thickness ($1/l_C$) to the melting point onset (Temperature). The closed diamonds and circles correspond to SAXS based crystal thickness estimates for the *syn* and *meso* samples respectively. The open symbols correspond to crystal thickness values calculated from an integer times the length of a repeat unit. The numerical labels added to the vertical lines that rise form these $1/l_C$ values correspond to the related number of repeats. The black line represents the melting point for extended chain crystals whereas the red line is related to the melting of folded chain crystals.

The red line connects all melting points (onset melting point obtained from the WAXD crystallinity evolution) of the *meso* sample (open circles) and suggests that the melting point at 45.6 °C during the first heating run is due to crystals that are only two molecular repeats thick. The other two melting points at 74.6 and 94.0 °C are due to the melting of crystals that are 3 and 4 molecular repeats thick as experimentally confirmed by SAXS.

The black line connects three of the five melting points found in the *syn* sample (open diamonds). These melting points were added to Figure 2 with dashed vertical lines and labelled with the number of molecular repeats along the crystal thickness. Two melting points of the *syn* sample could be better linked to the red line. They correspond to the melting of crystals that are 2 and 5 molecular repeats thick. These melting points are indicated with full vertical lines in Figure 2.

One may wonder why two Gibbs-Thomson lines are required to cover all crystal thickness / melting point relationships in Figure 6. The equilibrium melting points (intercepts of the graphs) of both crystal types are equal, implying that the $\Delta H/\Delta S$ ratios (defining T_m^0) of both crystal types are also identical. ΔS represents the entropy of melting. It would be a huge coincidence that two fully random $\Delta H/\Delta S$ ratios would lead to exactly the same melting point. Therefore it is more likely that both ΔH and ΔS are identical for the two crystal types. With ΔH being equal, only a difference in σ_e can account for the two different slopes in the Gibbs Thomson plots of crystals. It is suggested that the steeper slope (larger σ_e value) corresponds to the melting points of folded chain crystals and the shallower slope (smaller σ_e value) to the melting points of extended chain crystals. To occurrence of folded and extended chain crystal lines with a common intercept is expected for crystals of the same polymer (with a given unit cell type). The unexpected element in the present case is that the two lines are identical for the *syn* and *meso* polymers (and oligomers), implying that the surface energies and melting enthalpies and entropies of the two different species are very close, if not identical, although the crystal unit cells are different (because of molecular differences).

Following this line of thinking, the *meso* sample only contains chain folded crystals whereas the *syn* sample is predominantly composed out of extended chain crystals with in addition some 5 and 2 molecular repeat thick folded chain crystals. This makes sense given the lower molecular weight of the *syn* oligomer (Table 3).

Based on this analysis, the melting point of the folded chain lamellar crystallites of (long) polymers from the *meso* and *syn* moieties are not expected to be different. With similar σ_e, ΔH and ΔS (and hence T_m^0) values and with identical glass transition temperatures (see Figure S12) one cannot expect a hugely different crystallization and melting behavior. This is in fact what experimentally is observed (see Figure S12). As the glass transition temperature of the oligomers should be lower than the polymer value (14 °C) and as the proximity of the glass transition temperature does not impede crystallization in the polymer cases, one has to accept another reason for inhibited crystallization of the *meso* oligomer. It is suggested that the slower crystallization kinetics for the *meso* oligomers might be due a stronger tendency to adopt gauche configurations, which might hamper nucleation. Apparently, such effects no longer affect the crystallization kinetics when high molecular weight polymers crystallize into larger crystals.

Conclusion

Polyesters were synthesized from dimethyl succinate and four different diols namely, 1,4-butanediol, *meso* and *rac-syn*-2,3-difluorobutanediol, and 2,2,3,3,-tetrafluorobutanediol. While the polymerization was optimized to obtain high molecular weight polymers, the characterization was focused on the differences and similarities of the thermal and scattering behaviour of two novel fluoride containing polyesters derived from *meso* and *rac-syn* 2,3-fluorobutanediol. In this context, the interplay of the relative configuration of diastereomeric vicinal difluoride groups on the conformational properties of polymers was investigated. First, a *syn* and *meso* vicinal fluoride containing diol were successfully incorporated in the polyester chain as confirmed by ^{1}H, ^{13}C and ^{19}F NMR analysis. Molecular weight values ranged between 25 and 30 kDa, after optimization of the polymerization method. The thermal behaviour of these polymers was found to be virtually identical, although differences were anticipated based on differences in preferred chain configuration. Oligomers of these *syn* and *meso* polymers did, however, display differences in thermal behaviour, with the *meso* species displaying a lower propensity towards crystallization.

The thermal behaviour of the polyester oligomers in relation to their semi-crystalline structure was thoroughly investigated using time-resolved synchrotron SAXS and WAXD. From these measurements, it could be concluded that the incorporation of *rac-syn* and *meso* vicinal fluoride units in the polymer chain both resulted in semi-crystalline oligomers with around 50% crystallinity but that the populations of chain folded and extended chain crystals were different. Based on a Gibbs Thomson analysis relating crystal sizes to melting points, it could be deduced that the *syn* and *meso* oligomers and polymers have the same equilibrium melting points and enthalpies. It therefore seems that the slower crystallization kinetics for the *meso* oligomers might be due a stronger tendency to adopt gauche configurations, which hampers crystal nucleation. Apparently, such effects no longer affect the crystallization kinetics when high molecular weight polymers crystallize into larger crystals.

Acknowledgements

S.L. acknowledges the Flanders Innovation & Entrepreneurship agency (VLAIO) for the funding of her PhD fellowship. R.S thanks the University of Southampton for funding.

References

1. Reiss-Nunes, R. C.; Riande, E.; Guzmán, J.; Chavez, N. A., Stress Optical Behavior of Partially Fluorinated Aliphatic Polyesters. *Macromol.* **2000,** *33* (25), 9464-9467.
2. Plunkett, R. J. Tetrafluoroethylene polymers. 1941.
3. Antonucci, J. M., New Monomers for Use in Dentistry. In *Biomedical and Dental Applications of Polymers*, Gebelein, C. G.; Koblitz, F. F., Eds. Springer US: Boston, MA, 1981; pp 357-371.
4. Trischler, F. D.; Hollander, J., Thermally stable polymers. *J. Polym. Sci., Part A-1: Polym. Chem.* **1969,** *7*, 971-975.
5. Yoon, S. C.; Ratner, B. D., Surface-structure of segmented poly(ether urethanes) and poly(ether urethane ureas) with various perfluorochain extenders- and X-ray photoelectron spectroscopic investigation. *Macromol.* **1986,** *19* (4), 1068-1079.
6. Honeychuck, R. V.; Ho, T.; Wynne, K. J.; Nissan, R. A., Preparation and characterization of polyurethanes based on a series of fluorinated diols. *Chem. Mater.* **1993,** *5* (9), 1299-1306.
7. Mera, A. E.; Griffith, J. R., Melt condensation and solution polymerization of highly fluorinated aliphatic polyesters. *J. Fluorine Chem.* **1994,** *69* (2), 151-155.
8. Schweiker, G. C.; Robitschek, P., Condensation polymers containing fluorine. 1. Synthesis of linear polyesters from fluorine-containing diols. *J. Polym. Sci.* **1957,** *24* (105), 33-41.
9. Trischler, F. D.; Hollander, J., Thermally stable polyesters. *J. Polym. Sci., Part A-1: Polym. Chem.* **1969,** *7*, 971-975.
10. Johncock, P.; Barnett, S. P.; Rickard, P. A., Preparation and some properties of 2,2,6,6-tetrahydryl-F-heptanedioic acid and its polyester with 1,1,5,5,-tetrahydryl-F-1,5-pentanediol. *J. Polym. Sci., Part A-1: Polym. Chem.* **1986,** *24* (9), 2033-2045.
11. Reis-Nunes, R. C.; Riande, E.; Chavez, N. C.; Guzmán, J., Comparative Study of the Conformational Characteristics of Partially Fluorinated Polyesters and Their Hydrogenated Counterparts. *Macromol.* **1996,** *29* (24), 7989-7994.
12. Hudlicky, M., *Organic Fluorine Chemistry*. Plenum: New York, 1971.
13. Natta, G., Une nouvelle classe de polymères D alpha-olefins ayant une regularité de structure exceptionelle. *J. Polym. Sci.* **1955,** *16* (82), 143-154.
14. Natta, G., Polymers isotactiques. *Makromol. Chem.* **1955,** *16* (3), 213-237.

15. Natta, G.; Pino, P.; Corradini, P.; Danusso, F.; Mantica, E.; Mazzanti, G.; Moraglio, G., Crystalline high polymers of alpha-olefins. *J. Am. Chem. Soc.* **1955,** *77* (6), 1708-1710.
16. Hunter, L., The C–F bond as a conformational tool in organic and biological chemistry. *Beilstein Journal of Organic Chemistry* **2010,** *6*, 38.
17. Thiehoff, C.; Rey, Y. P.; Gilmour, R., The Fluorine Gauche Effect: A Brief History. *Israel Journal of Chemistry* **2017,** *57* (1-2), 92-100.
18. Buissonneaud, D. Y.; van Mourik, T.; O'Hagan, D., A DFT study on the origin of the fluorine gauche effect in substituted fluoroethanes. *Tetrahedron* **2010,** *66* (12), 2196-2202.
19. Craig, N. C.; Chen, A.; Suh, K. H.; Klee, S.; Mellau, G. C.; Winnewisser, B. P.; Winnewisser, M., Contribution to the Study of the Gauche Effect. The Complete Structure of the Anti Rotamer of 1,2-Difluoroethane. *J. Am. Chem. Soc.* **1997,** *119* (20), 4789-4790.
20. Dixon, D. A.; Smart, B. E., Electronic structure and conformational analysis of 1,2-difluoroethane. *J. Phys. Chem.* **1988,** *92* (10), 2729-2733.
21. Franco, M. L.; Ferreira, D. E. C.; Santos, H. F. D.; De Almeida, W. B., Ab Initio Highly Correlated Conformational Analysis of 1,2-Difluorethane and 1,2-Dichloroethane. *J. Chem. Theory Comput.* **2008,** *4* (5), 728-739.
22. Durig, J. R.; Liu, J.; Little, T. S.; Kalasinsky, V. F., Conformational analysis, barriers to internal rotation, vibrational assignment, and ab initio calculations of 1,2-difluoroethane. *J. Phys. Chem.* **1992,** *96* (21), 8224-8233.
23. Fox, S. J.; Gourdain, S.; Coulthurst, A.; Fox, C.; Kuprov, I.; Essex, J. W.; Skylaris, C.-K.; Linclau, B., A Computational Study of Vicinal Fluorination in 2,3-Difluorobutane: Implications for Conformational Control in Alkane Chains. *Chem. Eur. J.* **2015,** *21* (4), 1682-1691.
24. Wang, Y.; Kirsch, P.; Lebl, T.; Slawin, A. M. Z.; O'Hagan, D., The preferred conformation of erythro- and threo-1,2-difluorocyclododecanes. *Beilstein Journal of Organic Chemistry* **2012,** *8*, 1271-1278.
25. Tavasli, M.; O'Hagan, D.; Pearson, C.; Petty, M. C., The fluorine gauche effect. Langmuir isotherms report the relative conformational stability of (±)-erythro- and (±)-threo-9,10-difluorostearic acids. *Chem. Commun.* **2002,** (11), 1226-1227.
26. Hamatani, T.; Matsubara, S.; Matsuda, H.; Schlosser, M., A stereocontrolled access to vicinal difluoroalkanes. *Tetrahedron* **1988,** *44* (10), 2875-2881.
27. Rozen, S.; Brand, M., Direct addition of elemental fluorine to double bonds. *The Journal of Organic Chemistry* **1986,** *51* (19), 3607-3611.
28. Kirsch, P., Fluorine in liquid crystal design for display applications. *Journal of Fluorine Chemistry* **2015,** *177*, 29-36.
29. Kirsch, P.; Bremer, M., Understanding Fluorine Effects in Liquid Crystals. *ChemPhysChem* **2010,** *11* (2), 357-360.
30. Hunter, L., The C–F bond as a conformational tool in organic and biological chemistry. *Beilstein J. Org. Chem.* **2010,** *6* (38).
31. Zimmer, L. E.; Sparr, C.; Gilmour, R., Konformative Fluoreffekte in der Organokatalyse: eine neuartige Strategie zum molekularen Design. *Angew. Chem.* **2011,** *123* (50), 12062-12074.
32. O'Hagan, D., Understanding organofluorine chemistry. An introduction to the C-F bond. *Chem. Soc. Rev.* **2008,** *37* (2), 308-319.
33. Aufiero, M.; Gilmour, R., Informing Molecular Design by Stereoelectronic Theory: The Fluorine Gauche Effect in Catalysis. *Accounts of Chemical Research* **2018,** *51* (7), 1701-1710.
34. Linclau, B.; Leung, L.; Nonnenmacher, J.; Tizzard, G., Synthesis and crystallographic analysis of meso-2,3-difluoro-1,4-butanediol and meso-1,4-dibenzyloxy-2,3-difluorobutane. *Beilstein J Org Chem* **2010,** *6*, 62.

35. Szpera, R.; Kovalenko, N.; Natarajan, K.; Paillard, N.; Linclau, B., The synthesis of the 2,3-difluorobutan-1,4-diol diastereomers. *Beilstein Journal of Organic Chemistry* **2017,** *13*, 2883-2887.
36. Alksnis, A.; Deme, D.; Surna, J., Synthesis of oligoesters and polyesters from oxalic acid and ethylene glycol. *J. Polym. Sci., Polym. Chem. Ed.* **1977,** *15* (8), 1855-1862.
37. Jacquel, N.; Freyermouth, F.; Fenouillot, F.; Rousseau, A.; Pascault, J. P.; Fuertes, P.; Saint-Loup, R., Synthesis and properties of poly (butylene succinate): Efficiency of different transesterification catalysts. *J. Polym. Sci., Part A-1: Polym. Chem.* **2011,** *49* (24), 5301-5312.
38. Lavilla, C.; Alla, A.; de Ilarduya, A. M.; Munoz-Guerra, S., High Tg Bio-Based Aliphatic Polyesters from Bicyclic D-Mannitol. *Biomacromol.* **2013,** *14* (3), 781-793.
39. Zakharova, E.; Lavilla, C.; Alla, A.; Martínez de Ilarduya, A.; Muñoz-Guerra, S., Modification of properties of poly(butylene succinate) by copolymerization with tartaric acid-based monomers. *Eur. Polym. J.* **2014,** *61*, 263-273.
40. Elizalde, L. E.; de los Santos-Villarreal, G.; Santiago-García, J. L.; Aguilar-Vega, M., Step-Growth Polymerization. In *Handbook of Polymer Synthesis, Characterization, and Processing*, John Wiley & Sons, Inc.: 2013; pp 41-63.
41. Hosemann, R.; Bagchi, S. N., *Direct analysis of diffraction by matter* North Holland Publishing Co, Amsterdam: 1962.

Table of content

Conformational influence of fluorinated building blocks on the physical properties of polyesters

Sophie Lingier, Robert Szpera, Bart Goderis, Bruno J. Linclau, Filip E. Du Prez